Supplemental Material

Genotyping

For genotyping, genomic DNA was collected from mouse tails and digested overnight with protease K. A 1033-bp region of Myo1c flanking the mutated codon 61 by 469 and 564 bp was amplified using primers gcattccagcatcctgcaacc and cagtgtcagccactgcaaacc. PCR products were digested with *Bam*H I to distinguish mutant from wild-type alleles, as the Y61G mutagenesis introduced a *Bam*H I restriction site. Predicted product sizes for each genotype were: homozygous wild-type - 1033 bp; heterozygotes - 1033, 564, and 469 bp; homozygous mutants – 564 and 469 bp.

Myo1c detection

We generated an antibody selective for the Y61G mutant Myo1c by immunizing rabbits with a peptide containing the Y61G substitution (CGGGNPYRDLQI**G**SRQHMERYR, where CGGG was added for column conjugation). Antisera were passed over a column constructed with the wild-type peptide (CGGGNPYRDLQI**Y**SRQHMERYR); the flow-through was applied to a column constructed with the mutant peptide. Specific antibodies were eluted with acid and base, neutralized, and concentrated. Using immunoblots with purified rat wild-type or Y61G Myo1c, we found that >100-fold more wild-type protein was required to generate a band with equal intensity to that with Y61G-Myo1c.

Proteins were extracted from mouse tissues using solutions containing 1% SDS; protein concentrations were measured using the bicinchoninic acid assay (Pierce). Equal amounts of wild-type or Y61G extracts were separated by SDS-PAGE and transferred to Immobilon P membranes (Millipore). Immunoblot detection was as previously described (Holt et al., 2002). Other methods were as described previously (Gillespie et al., 1999; Holt et al., 2002).

Data analysis

A list of the most important variables used in our analysis is presented in Table 1. We used the inferred-shift method of Shepherd and Corey (1994) to calculate the adaptive shift of the current-displacement curve during sustained mechanical displacements (Hirono et al., 2004). The method is illustrated in Supplemental Figure 1C.

An instantaneous current-displacement curve was calculated from the maximal transduction currents measured from a family of displacements, and then fit with a three-state Boltzmann model:

$$I = I_{closed} - \frac{I_{max}}{1+\exp[Z_2 \cdot (X_s - X_{02})/kT] \cdot (1+\exp[Z_1 \cdot (X_s - X_{01})/kT])} \quad \text{(S2)}$$

where Z_1 and Z_2, the single-channel gating forces, X_{01} and X_{02}, the midpoints along the displacement axis for the two transitions, I, the transduction current at any given time, I_{closed}, the membrane current when all transduction channels are closed, and I_{max}, the maximum transduction current. For each current record, evoked by a given stimulus X_s, the adaptive shift X_e was calculated by solving the following three-state Boltzmann equation for X_e using Mathematica 4.0 or 5.0:

$$I = I_{closed} - \frac{I_{max}}{1+\exp[Z_2 \cdot (X_s - X_{02} - X_e)/kT] \cdot (1+\exp[Z_1 \cdot (X_s - X_{01} - X_e)/kT])} \quad \text{(S3)}$$

We eliminated points derived from regions in which the slope of the current-displacement relation was less than 5% of the maximum slope (Hirono et al., 2004).

To extract fast and slow adaptation parameters, plots of $X_e(t)$ were fit with double-exponential functions of the following form:

$$X_e = X_{e(fast)} \cdot (1 - e^{-t/\tau_{fast}}) + X_{e(slow)} \cdot (1 - e^{-t/\tau_{slow}}) \quad \text{(S4)}$$

When slow-adaptation time constants were very large and amplitudes small, we excluded those values of τ_{slow}. We used an iterative process of supplying estimates for the values of fast and slow extent and τ, judging the best fit by minimizing χ^2. Unlike our previous work (Hirono et al., 2004), we calculated independent fast and slow time constants for each X_s (Supplemental Material and Supplemental Figure 1).

To compare and contrast rates of fast and slow adaptation of individual cells, we linearly fit X_s-rate plots; the slope is the rate constant. In addition, we generated a dataset with averaged extent, τ, and rates as a function of X_s. The dependence of fast extent on displacement was fit by:

$$X_{e(fast)} = X_{e(fast)\infty} \cdot \frac{P_o - P_{o(rest)}}{1 - P_{o(rest)}} \quad \text{(S5)}$$

where P_o is the open probability at a given displacement and $P_{o(rest)}$ is the open probability at rest. This equation suggests that the maximal extent of fast adaptation is a constant, but its extent for any given displacement depends on P_o, weighted for its rest value. In turn, we implicitly assume that the Ca^{2+} concentration in the stereocilium is proportional to P_o, which is a reasonable approximation (Lumpkin and Hudspeth, 1998).

Time constant data for fast adaptation were fit with the following equation, derived from transition-state rate theory (Howard, 2001):

$$\tau_{fast} = \frac{1}{k_1 + k_2^0 \exp\left[\frac{\gamma X_s \kappa_g \Delta x_a}{kT}\right]} \tag{S6}$$

where k_1 is the rate of the displacement-independent component, k_2^0 is the displacement-dependent rate in the absence of displacement, κ_g is the stiffness of a single gating spring, and Δx_a is the mechanical movement required for displacement-dependent rate acceleration.

The extent of slow adaptation was calculated using:

$$X_{e(slow)} = X'_{e(total)} \cdot X_s - X_{e(fast)} \tag{S7}$$

This equation assumes that the extent of slow adaptation equals the total extent of adaptation (the first term) minus the extent of fast adaptation.

The rate constant for slow adaptation (k_{slow}) was determined by fitting rate-displacement data with:

$$Rate = k_{slow} \cdot (X'_{e(total)} \cdot X_s - X_{e(fast)}) \tag{S8}$$

The negative term reflects release and the scaling by $X'_{e(total)}$ reflects the distribution of force between the extent spring (Shepherd and Corey, 1994) and adaptation motor.

Maximal transduction currents were converted to open probabilities using $P_o = (I + I_{closed})/I_{max}$. We fit the average displacement-P_o plots of Figs. 2C,I with:

$$P_{open} = \frac{1}{1 + \exp[Z_2 \cdot (X_s - X_{02})/kT] \cdot (1 + \exp[Z_1 \cdot (X_s - X_{01})/kT])} \tag{S9}$$

Simple displacement shift of the current-displacement curve describes adaptation in frog and mouse hair cells

The inferred-shift analysis assumes that during adaptation the shape of the current-displacement curve remains unchanged, only shifting along the x-axis. To confirm that a pure x-axis shift occurs in frog and mouse vestibular hair cells, we generated current-displacement curves before and after adapting pulses that elicit full fast adaptation and partial slow adaptation. As previously noted, a pure x-axis shift fit the data well (Supplemental Figure 1A,B). Although we did not specifically examine the current-displacement curve immediately after fast adaptation, it seems very unlikely that its slope would change significantly in the first few milliseconds, then quickly revert to the control slope. Confirming that suggestion, Cheung and Corey (2005) found that adaptation in frog saccule hair cells that took place within 3 ms of the onset of a stimulus was described well by a pure shift. We thus believe that the assumptions used in the inferred-shift analysis are justified by the behavior of transduction and adaptation in these hair cells. The procedure for the inferred-shift method is described in Supplemental Figure 1C.

Optimal fitting of $X_e(t)$ plots

We initially assumed that the time constants for fast and slow adaptation did not depend on stimulus amplitude; accordingly, we fit sets of $X_e(t)$ plots assuming the presence of two exponential components with single fast and slow time constants. We found that the fits deviated slightly from the data points, however, particularly for the largest displacements. To determine the optimal method for fitting the data, we therefore averaged $X_e(t)$ datasets from 15 frog or 9 mouse hair cells, then fit them with three models. The first model assumed that single exponential functions, with τ values that varied with displacement, fit the data (16 parameters for frog or 20 parameters for mouse in the dataset). The second model assumed only two time constants, as above (18 or 24 parameters in the dataset), while the third model assumed that the fast and slow time constants varied depending on the stimulus amplitude (32 or 40 parameters in the dataset).

In both frog (Supplemental Figure 2, top) and mouse (Supplemental Figure 2, bottom) hair cells, the adaptive shift was fit more accurately by allowing the time constants to vary with stimulus amplitude. The better fit of this model is seen in the residuals plot; with two time constants, the $X_e(t)$ data points of the largest stimulus (red) systematically deviate from zero, particularly at early time points. We therefore fit $X_e(t)$ datasets from individual cells with two varying time constants and two amplitudes per displacement.

Supplemental Table

Supplemental Table 1. **Variables used.**

Variable	**Definition**
X_s	Mechanical displacement applied to hair bundle's tip
$X_e(t)$	Extent of adaptation at time t determined by inferred-shift analysis
$X_{e(fast)}$	Maximum extent of fast adaptation for a given X_s
$X_{e(slow)}$	Maximum extent of slow adaptation for a given X_s
$X_{e(fast)\infty}$	Maximum extent of fast adaptation extrapolated to infinite X_s
τ_{fast}	Time constant for fast adaptation for a given X_s
τ_{slow}	Time constant for slow adaptation for a given X_s
$X'_{e(fast)}$	Slope of the displacement-extent relation for fast adaptation
$X'_{e(slow)}$	Slope of the displacement-extent relation for slow adaptation

Supplemental Figures

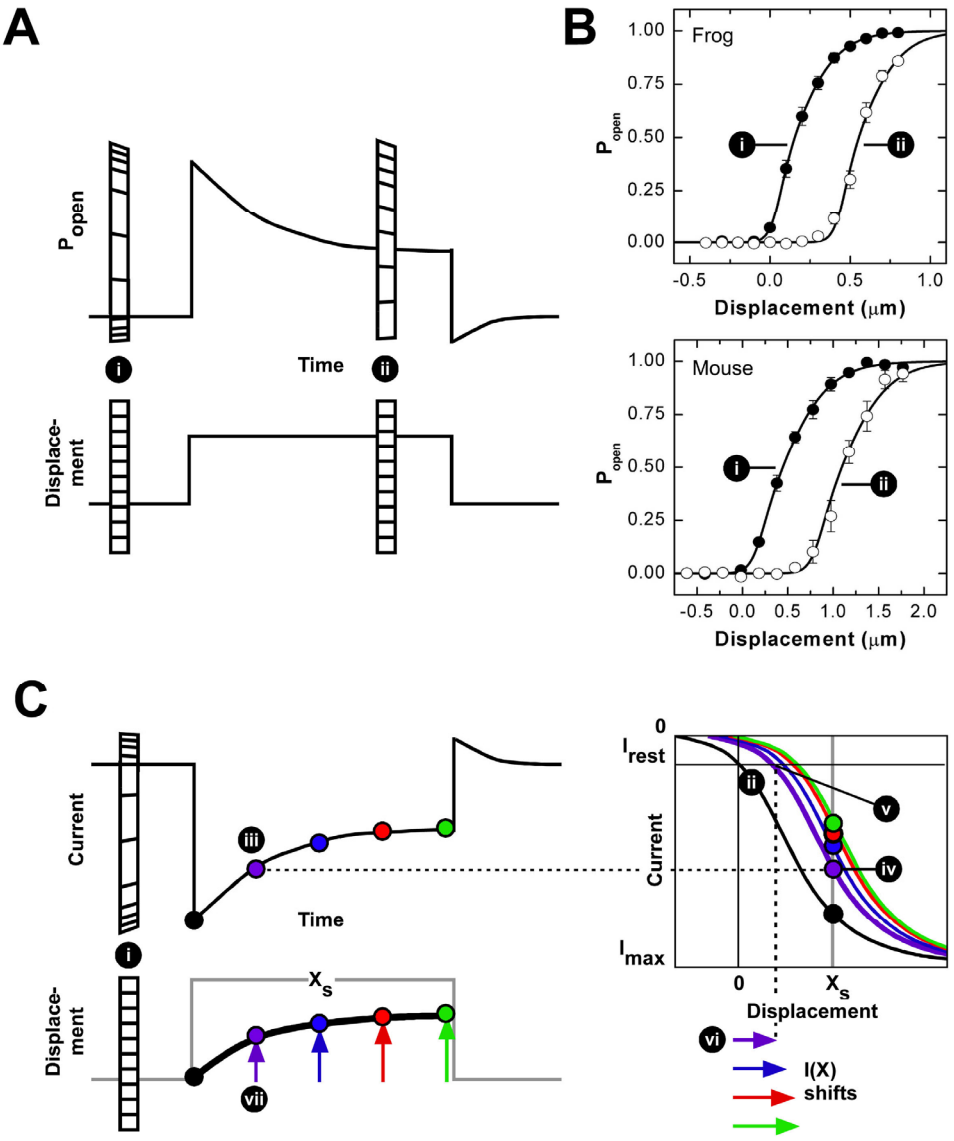

Supplemental Figure 1. **Determining the extent of adaptation.**

A: Protocol for measuring adaptive shift at a given time following an adapting pulse. At (i), a family of displacements is given, which allows generation of an initial $P_O(X)$ curve (P_O as a function of displacement). An adapting step is applied, and at some time t following its start, a new family of displacements is applied at (ii). The resulting P_O values are used to generate an adapted $P_O(X)$ curve.

B: Justification for the inferred shift method. Data generated using protocols similar to those in A; (i) and (ii) refer respectively to $P_O(X)$ curves before and during adaptation pulse. Current-displacement relationships were determined before and after 50-ms, 0.4 μm (frog) or 150 ms, 1.0 μm (mouse) adapting pulses. The parameters from the three-state Boltzmann fits to the initial current-displacement data were used to fit the post-adaptation current-displacement data, allowing a pure displacement shift along the x-axis. Data were averaged from 15 (frog) or 3 (mouse) cells; $P_O(X)$ curves were employed to allow comparison between cells of different maximal current amplitude.

C: Inferred-shift method. Currents are plotted instead of P_O to allow comparison to data (e.g., Figures 2 and 6). A family of displacements (i) allows measurement of a current-displacement curve, which is plotted in (ii). During an adapting pulse, each transduction-current data point is analyzed identically. Taking the purple point (iii) as an example, the point is plotted on the current-displacement plot using the stimulus displacement (X_S) for the x-axis (iv). The initial current-displacement curve (ii) is then shifted along the displacement axis until it intercepts this point, generating the shifted curve (v). The amount of shift of the current-displacement curve (vi) corresponds to $X_e(t)$, the adaptive shift at time t. This value is then plotted on a X_e – t plot (vii), shown here superimposed on the stimulus template to emphasize incomplete adaptation.

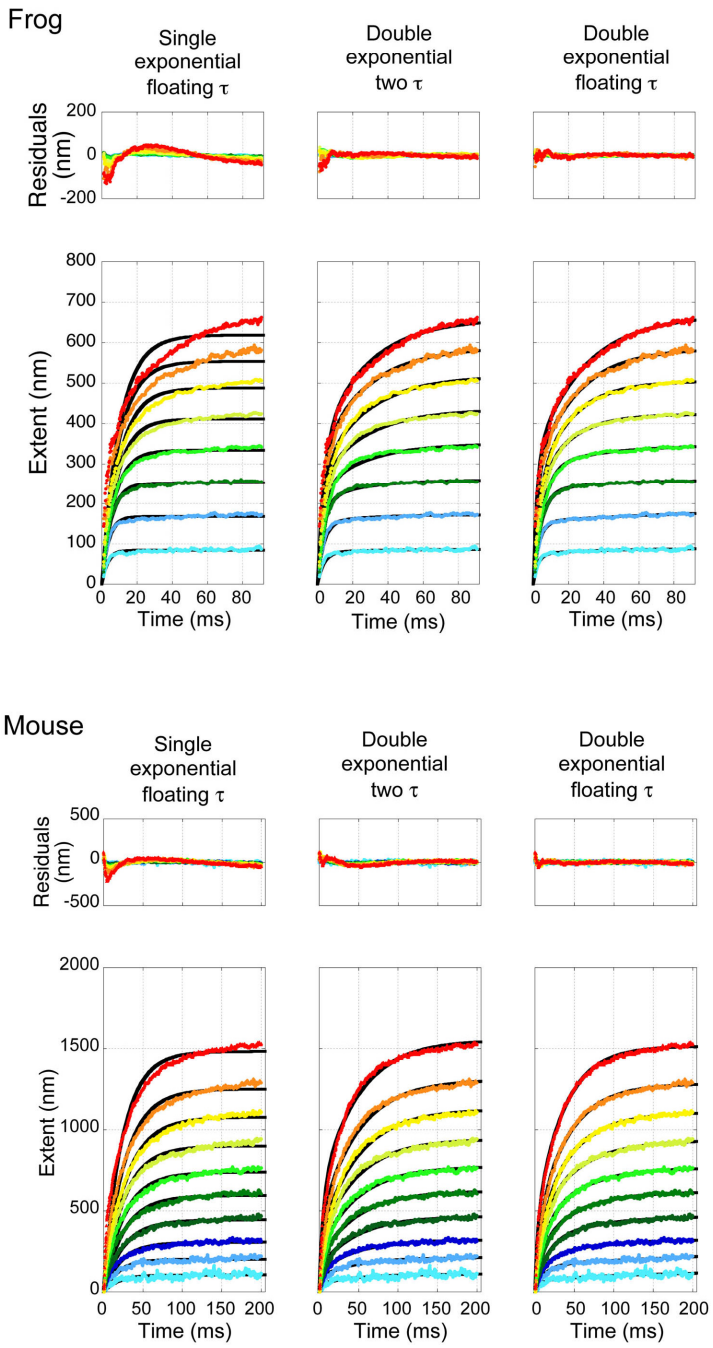

Supplemental Figure 2. **Fitting $X_e(t)$ plots with three models.**

$X_e(t)$ data was averaged across frog (top) and mouse (bottom) datasets, then was fit independently with three models. Left, X_e – t plots for each displacement were fit with single exponential functions. Middle, all X_e – t plots were fit simultaneously with two time constants for the entire dataset and two floating amplitudes for each displacement. Right, X_e – t plots were fit

individually with two time constants and two final amplitudes. Residuals plots show the difference between the fits and the data points. The residuals are minimal for both frog and mouse with the model on the right.

Supplemental References

Howard, J. (2001). Mechanics of Motor Proteins and the Cytoskeleton (Sunderlaand, MA: Sinauer Associates).

Lumpkin, E. A., and Hudspeth, A. J. (1998). Regulation of free Ca^{2+} concentration in hair-cell stereocilia. J. Neurosci. 18, 6300-6318.